XIII SIMMEC
Simpósio de Mecânica Computacional
29 de Outubro a 1º de Novembro de 2018
UFES - Campus Goiabeiras - Vitória, ES

Uma Estratégia MFS Eficiente para Prever o Desempenho Acústico de Barreiras Finas em Forma de T

An Efficient MFS strategy for Predicting the Acoustic Performance of T-shaped Thin Barriers

Edmundo G. de A. Costa (1); Luís Godinho (2); José A. F. Santiago (3); Webe J. Mansur (4); Franciane C. Peters (5)

(1) Dr. Engenheiro Civil, COPPE - Universidade Federal do Rio de Janeiro, Rio de Janeiro - RJ, Brasil.
(2) Dr. Prof., ISISE - Universidade de Coimbra, Coimbra - PT, Portugal.
(3) Dr. Prof., COPPE - Universidade Federal do Rio de Janeiro, Rio de Janeiro - RJ, Brasil.
(4) Dr. Prof., COPPE - Universidade Federal do Rio de Janeiro, Rio de Janeiro - RJ, Brasil.
(5) Dra. Profa., COPPE - Universidade Federal do Rio de Janeiro, Rio de Janeiro - RJ, Brasil.
Email para Correspondência: edmundo_costa@coc.ufrj.br; (1) Apresentador

Resumo: Neste artigo, uma estratégia MFS no domínio da frequência é aplicada para avaliar o campo sonoro gerado por uma fonte linear na presença de barreiras finas em forma de T. A formulação proposta é desenvolvida utilizando funções de Green definidas através do método das imagens, permitindo um custo computacional reduzido do modelo numérico. Tanto o solo quanto o edifício são simulados como superfícies planas rígidas infinitas, e a barreira acústica é tratada como sendo absorvente. O tratamento de superfície das barreiras é caracterizado por um material absorvente poroso. O modelo de Zwikker e Kosten é aqui usado para calcular as propriedades do material poroso. Para validar a implementação numérica do método proposto, os resultados são comparados com soluções da formulação Dual-BEM. Simulações numéricas são realizadas a fim de demonstrar a eficiência da formulação proposta e o desempenho acústico das barreiras finas em forma de T em cenários típicos de ruído de tráfego. Os resultados mostrarão que o MFS pode ser uma ferramenta muito interessante para prever o desempenho acústico de barreiras finas com formas complexas e condições de contorno complicadas.

Palavras chaves: Formulação MFS; formulação Dual-BEM; funções de Green; barreiras finas em forma de T; modelo de Zwikker e Kosten; material absorvente poroso.

Abstract: In this paper, a frequency-domain MFS strategy is applied to evaluate the sound field generated by a linear source in the presence of T-shaped thin barriers. The proposed formulation is developed by making use of Green's functions defined by using the image-source technique, allowing a reduced computational cost of the numerical

model. Both the ground and the building are simulated as infinite rigid plane surfaces, and the acoustic barrier is assumed to be absorptive. The surface treatment of the barriers is characterized by a porous absorbent material. The Zwikker and Kosten model is here used for predicting the properties of the porous material. To validate the numerical implementation of the proposed method, the results are compared with solutions of the Dual-BEM formulation. Numerical simulations are carried out in order to demonstrate the efficiency of the proposed formulation, and the acoustic performance of the T-shaped thin barriers in typical scenarios of traffic noise. The results will show that the MFS could be a very interesting tool for predicting the acoustic performance of thin barriers with complex shapes and complicated boundary conditions.

Keywords: MFS formulation; Dual-BEM formulation; Green's functions; T-shaped thin barriers; Zwikker and Kosten model; porous absorbent material.

1 INTRODUCTION

Several empirical and numerical methods have been widely used to simulate and analyse acoustic wave propagation around the acoustic barriers. Among these, the Boundary Element Method (BEM) allows an efficient analysis of acoustic barriers of complex shapes and complicated boundary conditions. The BEM has a number of advantages over other methods (Brebbia, 1984). However, the boundary integral equation formulation presents some difficulties for analysis of very thin bodies, in the form of near-singularities and near-degeneracy of the final system of equations.

Filippi and Dumery (1969) and Cassot (1975) developed an efficient boundary integral equation technique to analyse the scattering of waves by thin rigid screens in infinite domain. Later, Kawai and Terai (1990) combined the standard and hyper-singular integral equations to predict the outdoor sound propagation and its attenuation by thin absorbing barriers over a rigid ground and avoided discretization of the infinite plane by making use of a Green's function obtained by means of the image-source technique. This formulation, which combines the use of standard and hyper-singular integral equations over a thin body, would later be called the Dual-BEM formulation.

More recently, meshless methods have attracted great interest of scientists and researchers for acoustics engineering problems. The Method of Fundamental Solution (MFS) is one of these methods and its mathematical formulation is quite simple. It is also based on the prior knowledge of fundamental solutions, but not requiring the numerical and analytical integrations that need to be performed in the BEM. In addition, it is also very well suited to the problems of infinite and semi-infinite domains since it automatically satisfies the Sommerfeld radiation condition. However, one disadvantage of the MFS is the determination of the position of the pseudo-boundary on which the singularities are placed. Therefore, Karageorghis (2009) has proposed a simple algorithm for estimating an optimal pseudo-boundary for certain boundary value problems. Costa *et al*. (2011, 2012), Godinho et al. (2012) and Costa *et al*. (2016, 2018)

have shown that, despite its simplicity, the MFS is a very interesting tool to efficiently predict sound wave propagation in the frequency domain.

This paper analyses the two-dimensional sound field around T-shaped thin acoustic barriers in the frequency-domain by means of the MFS. Here, the configurations analysed make use of the sub-region technique, and the Green's functions are employed for limiting the number of discretized surfaces and reducing the computational cost of the proposed model. In this model, both the ground and the tall building are modeled as infinite rigid plane surfaces, and the thin barriers are assumed to be absorptive. The surface treatment is characterized by a porous absorbent material. The properties of this material are computed by using the Zwikker and Kosten model. The proposed model is verified by the comparison of numerical results with a reference model based on the dual-BEM formulation. The advantages of the proposed model such as its stability and accuracy are also illustrated by performing comparisons with a reference model. The insertion loss is presented for T-shaped thin barriers with and without absorbent treatment, allowing evaluating the effect of the absorbent treatment of the barriers in the sound reduction near to the façade of a building.

2 MATHEMATICAL FORMULATION

2.1 Problem definition

Consider the problem of acoustic wave propagation in a region Ω of infinite extent along the *z*-direction in the presence of a T-shaped thin noise barrier over an infinite plane ground, as shown in Fig.1.

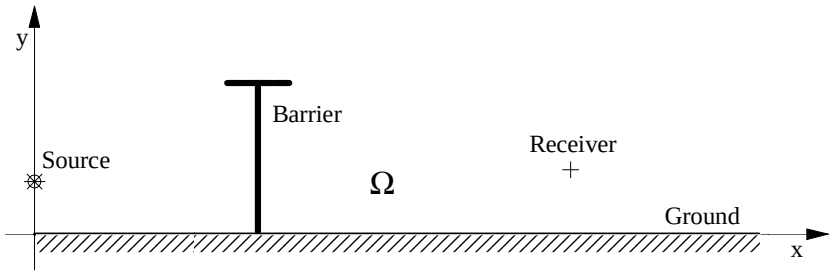

Figure 1. Geometry of the problem.

The propagation of an acoustic wave in the homogeneous linear fluid medium at rest is governed in the frequency domain by the Helmholtz equation, which can be written as:

$$\nabla^2 p(\mathbf{x}) + k^2 p(\mathbf{x}) = 0\,, \tag{1}$$

where $p(\mathbf{x})$ is the acoustic pressure, and $k = 2\pi f / c$ is the wave number, with f being the frequency and c the speed of sound in the acoustic medium.

Assuming an infinite domain excited by a harmonic point pressure source at position $\mathbf{x}_0$, the incident pressure field at any point $\mathbf{x}$ is given by:

$$p_{inc}(\mathbf{x},\mathbf{x}_0) = \frac{\mathrm{i}}{4} H_0^1(kr), \tag{2}$$

where $r = |\mathbf{x} - \mathbf{x}_0| = \sqrt{(x-x_0)^2 + (y-y_0)^2}$ and $H_0^1(\ldots)$ is the Hankel function of the first kind of order zero.

2.2 Green's functions

In analyses of acoustic wave propagation, the presence of totally reflecting plane surfaces can be taken into account by means of the image-source technique. Thus, considering an image source in relation to the horizontal axis *x*, as displayed in Fig. 2(a), the corresponding Green's function can be written as:

$$G(\mathbf{x},\mathbf{x}_0) = \frac{\mathrm{i}}{4}\left[H_0(kr_1) + H_0(kr_2) \right], \tag{3}$$

with $r_1 = \sqrt{(x-x_0)^2 + (y-y_0)^2}$ and $r_2 = \sqrt{(x-x_0)^2 + (y+y_0)^2}$.

This approach can be further extended to incorporate more reflecting surfaces. Thus, considering a quarter-space defined by two axes, one at *x* and other at *y*, as displayed in Fig. 2(b), the corresponding Green's function can be expressed as:

$$G(\mathbf{x},\mathbf{x}_0) = -\frac{\mathrm{i}}{4}\left[H_0(kr_1) + H_0(kr_2) + H_0(kr_3) + H_0(kr_4) \right], \tag{4}$$

with $r_3 = \sqrt{(x+x_0)^2 + (y-y_0)^2}$ and $r_4 = \sqrt{(x+x_0)^2 + (y+y_0)^2}$.

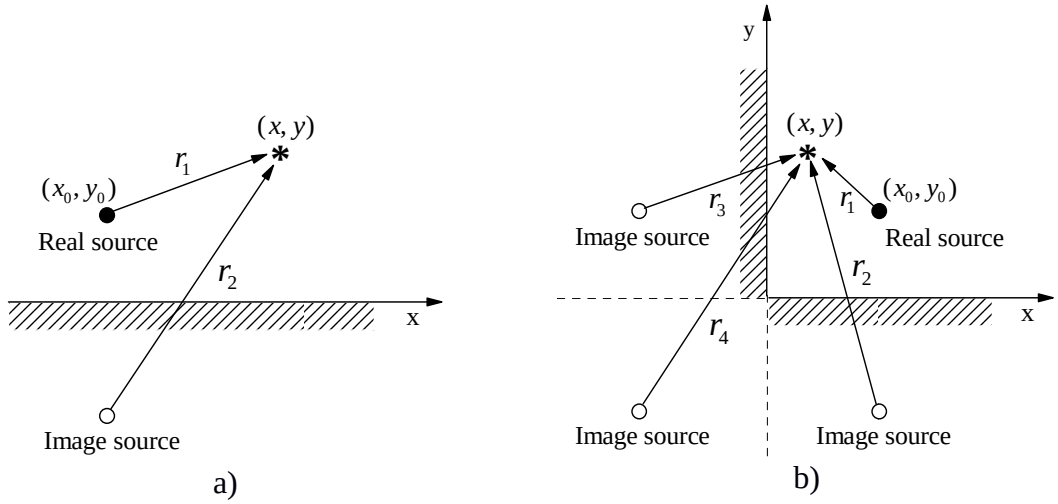

Figure 2. The image-source technique: a) Half-space and b) Quarter-space.

The above described Green's functions are only valid if the planes are totally rigid. However, it may be possible to account for partially-reflecting planes, multiplying the effect of the virtual sources by a generic reflection coefficient *R*. In this case, the Eqs. (3) and (4) become,

$$G(\mathbf{x},\mathbf{x}_0) = -\frac{\mathrm{i}}{4}\left[H_0(kr_1) + R_2 H_0(kr_2)\right], \tag{5}$$

$$G(\mathbf{x},\mathbf{x}_0) = -\frac{\mathrm{i}}{4}\left[H_0(kr_1) + R_2 H_0(kr_2) + R_3 H_0(kr_3) + R_2 R_3 H_0(kr_4)\right]. \tag{6}$$

The reflection coefficient is related to the impedance using the local reacting approximation (Salomons, 2001) given by:

$$R = \frac{Z\cos\theta - 1}{Z\cos\theta + 1}, \tag{7}$$

where *R* is the reflection angle.

In this study, the Zwikker and Kosten model is used for predicting the acoustic properties of the porous material and is defined by:

$$Z = \sqrt{\frac{c_s}{\Lambda^2} + i\frac{\sigma}{\Lambda\rho c}}. \tag{8}$$

where Λ is the porosity, c_s is the tortuosity (or structure factor), and σ is the flow resistivity.

3 THE METHOD OF FUNDAMENTAL SOLUTIONS

The MFS model is developed by assuming an acoustic domain divided into six sub-regions, as illustrated in Fig. 3, in which two special Green's functions are used. In this model, five circular interfaces are defined by using a number of collocation points (CP) and a number of virtual sources (VS) positioned outside each sub-region is also considered. Thus, within each sub-region, the MFS allows the acoustic field to be calculated as a linear combination of fundamental solutions, simulating the sound field within each sub-region by means of a set of virtual sources placed outside it and at a fixed distance from the circular interfaces limited by each sub-region.

For each sub-region, the acoustic pressure at an internal point $\mathbf{x}_k$ can then be written as:

$$p(\mathbf{x}_k) = \sum_{l=1}^{\mathrm{VS}_j} a_l^{\Omega_j} G_{kl}^{\Omega_j}(\mathbf{x}_k, \mathbf{x}_l^{\Omega_j}) + \delta_{IJ} G_{ks}^{\Omega_j}(\mathbf{x}_k, \mathbf{x}_s), \quad \text{within } \Omega_j\,(j=1,2,3), \tag{9}$$

$$p(\mathbf{x}_k) = \sum_{l=1}^{\mathrm{VS}_j} a_l^{\Omega_j} G_{kl}^{\Omega_j}(\mathbf{x}_k, \mathbf{x}_l^{\Omega_j}), \quad \text{within } \Omega_j\,(j=4,5,6), \tag{10}$$

and the normal component of the particle velocity as:

$$\frac{\partial p(\mathbf{x}_k)}{\partial \mathbf{n}} = \sum_{l=1}^{\mathrm{VS}_j} a_l^{\Omega_i} \frac{\partial G_{kl}^{\Omega_j}(\mathbf{x}_k, \mathbf{x}_l^{\Omega_j})}{\partial \mathbf{n}} + \delta_{IJ} \frac{\partial G_{ks}^{\Omega_j}(\mathbf{x}_k, \mathbf{x}_s)}{\partial \mathbf{n}}, \quad \text{within } \Omega_j\,(j=1,2,3), \tag{11}$$

$$\frac{\partial p(\mathbf{x}_k)}{\partial \mathbf{n}} = \sum_{l=1}^{\mathrm{VS}_j} a_l^{\Omega_j} \frac{\partial G_{kl}^{\Omega_j}(\mathbf{x}_k, \mathbf{x}_l^{\Omega_j})}{\partial \mathbf{n}}, \quad \text{within } \Omega_j\,(j=4,5,6), \tag{12}$$

where **n** is the unit normal vector pointing outwards of each sub-region (i.e. with opposing directions for each sub-region), $a_l^{\Omega_j}$ and $b_l^{\Omega_j}$ are the unknown amplitudes to be determined for each virtual source, $\mathbf{x}_k$ is the collocation point in which the continuity condition is enforced, $G_{ks}^{\Omega_j}(\mathbf{x}_k, \mathbf{x}_s)$ is the incident field regarding the acoustic pressure generated by the real source when placed in the sub-region Ω_j; $G_{kl}^{\Omega_j}(\mathbf{x}_k, \mathbf{x}_l^{\Omega_j})$ refers to the Green's function for the sub-region Ω_j, whose details were given in the previous section; *i* is the sub-region in which the real source is positioned and δ_{IJ} is the Kronecker delta.

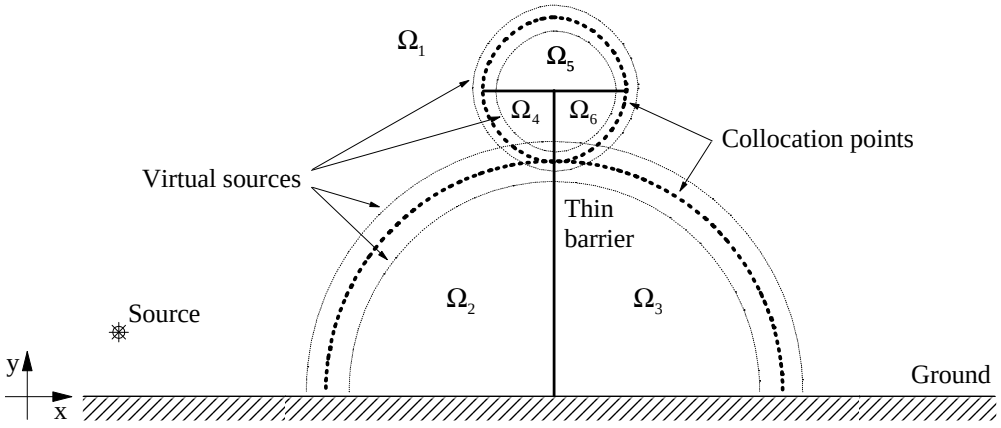

Figure 3. Schematic representation of the MFS model.

By imposing at each collocation point $\mathbf{x}_k$, continuity of the acoustic pressure and of the normal component of the particle velocity with respect to the circular interfaces, the following $2\mathrm{CP}\times 2\mathrm{VS}$ system of equations can be obtained:

$$\mathbf{A}\mathbf{x} = \mathbf{b}, \tag{13}$$

where

$$\mathbf{A}=\begin{bmatrix}
\mathbf{G}_{11}^{\Omega_1} & -\mathbf{G}_{12}^{\Omega_2} & \mathbf{0} & \mathbf{0} & \mathbf{0} & \mathbf{0} \\
\mathbf{H}_{11}^{\Omega_1} & -\mathbf{H}_{12}^{\Omega_2} & \mathbf{0} & \mathbf{0} & \mathbf{0} & \mathbf{0} \\
\mathbf{G}_{21}^{\Omega_1} & \mathbf{0} & -\mathbf{G}_{23}^{\Omega_3} & \mathbf{0} & \mathbf{0} & \mathbf{0} \\
\mathbf{H}_{21}^{\Omega_1} & \mathbf{0} & -\mathbf{H}_{23}^{\Omega_3} & \mathbf{0} & \mathbf{0} & \mathbf{0} \\
\mathbf{G}_{31}^{\Omega_1} & \mathbf{0} & \mathbf{0} & -\mathbf{G}_{34}^{\Omega_4} & \mathbf{0} & \mathbf{0} \\
\mathbf{H}_{31}^{\Omega_1} & \mathbf{0} & \mathbf{0} & -\mathbf{H}_{34}^{\Omega_4} & \mathbf{0} & \mathbf{0} \\
\mathbf{G}_{41}^{\Omega_1} & \mathbf{0} & \mathbf{0} & \mathbf{0} & -\mathbf{G}_{45}^{\Omega_5} & \mathbf{0} \\
\mathbf{H}_{41}^{\Omega_1} & \mathbf{0} & \mathbf{0} & \mathbf{0} & -\mathbf{H}_{45}^{\Omega_5} & \mathbf{0} \\
\mathbf{G}_{51}^{\Omega_1} & \mathbf{0} & \mathbf{0} & \mathbf{0} & \mathbf{0} & -\mathbf{G}_{56}^{\Omega_6} \\
\mathbf{H}_{51}^{\Omega_1} & \mathbf{0} & \mathbf{0} & \mathbf{0} & \mathbf{0} & -\mathbf{H}_{56}^{\Omega_6}
\end{bmatrix}, \tag{14}$$

with

$$\mathbf{G}_{kl}^{\Omega_l}=\begin{bmatrix}
G(\mathbf{x}_1,\mathbf{x}_1) & \cdots & G(\mathbf{x}_1,\mathbf{x}_{\mathrm{VS}_l}) \\
\vdots & \ddots & \vdots \\
G(\mathbf{x}_{\mathrm{CP}_k},\mathbf{x}_1) & \cdots & G(\mathbf{x}_{\mathrm{CP}_k},\mathbf{x}_{\mathrm{VS}_l})
\end{bmatrix}, \tag{15}$$

$$\mathbf{H}_{kl}^{\Omega_l}=\begin{bmatrix}
\dfrac{\partial G(\mathbf{x}_1,\mathbf{x}_1)}{\partial \mathbf{n}} & \cdots & \dfrac{\partial G(\mathbf{x}_1,\mathbf{x}_{\mathrm{VS}_l})}{\partial \mathbf{n}} \\
\vdots & \ddots & \vdots \\
\dfrac{\partial G(\mathbf{x}_{\mathrm{CP}_k},\mathbf{x}_1)}{\partial \mathbf{n}} & \cdots & \dfrac{\partial G(\mathbf{x}_{\mathrm{CP}_k},\mathbf{x}_{\mathrm{VS}_l})}{\partial \mathbf{n}}
\end{bmatrix}. \tag{16}$$

For example, if the real source is located in the region Ω_1, the unknown vector $\mathbf{x}$ is given by:

$$\mathbf{x}=\begin{bmatrix} a_1^{\Omega_1} & \cdots & a_{\mathrm{VS}_1}^{\Omega_1} & a_1^{\Omega_2} & \cdots & a_{\mathrm{VS}_2}^{\Omega_2} & \cdots & a_1^{\Omega_5} & \cdots & a_{VS_5}^{\Omega_5} & a_1^{\Omega_6} & \cdots & a_{VS_6}^{\Omega_6} \end{bmatrix}^T, \tag{17}$$

and right-hand-side term is defined as:

$$\mathbf{b}=\begin{bmatrix} -\mathbf{G}_1^{\Omega_1} & -\mathbf{H}_1^{\Omega_1} & -\mathbf{G}_2^{\Omega_1} & -\mathbf{H}_2^{\Omega_1} & -\mathbf{G}_3^{\Omega_1} & -\mathbf{H}_3^{\Omega_1} & -\mathbf{G}_4^{\Omega_1} & -\mathbf{H}_4^{\Omega_1} & -\mathbf{G}_5^{\Omega_1} & -\mathbf{H}_5^{\Omega_1} \end{bmatrix}^T, \tag{18}$$

$$\mathbf{G}_k^{\Omega_1}=\begin{bmatrix} G(\mathbf{x}_1,\mathbf{x}_s) & \cdots & G(\mathbf{x}_{\mathrm{CP}_k},\mathbf{x}_s) \end{bmatrix}, \tag{19}$$

$$\mathbf{H}_k^{\Omega_1}=\begin{bmatrix} \dfrac{\partial G(\mathbf{x}_1,\mathbf{x}_s)}{\partial \mathbf{n}} & \cdots & \dfrac{\partial G(\mathbf{x}_{\mathrm{CP}_k},\mathbf{x}_s)}{\partial \mathbf{n}} \end{bmatrix}. \tag{20}$$

Once this system of equations is solved, the acoustic pressure at any domain point may be obtained by using Eqs. (9) and (10).

4 MODEL VERIFICATION

In order to validate the numerical implementation of the proposed formulation, the results are compared with a reference solution based on Dual-BEM formulation. We consider a T-shaped thin barrier 5.0m tall located over a plane ground at (0.0m, 0.0m). The fluid medium is excited by a point source placed at position (-10.0m, 1.0m), as shown in Fig. 4. In this study, a cap 2.0m width was always considered. The acoustic medium is assumed to be air at 20 ^{o}C and atmospheric pressure of 1 atm, with density of 1.21 kg m^{-3} and sound propagation velocity of 343 m s^{-1}. Here, two test cases were analyzed. In the first test case, responses are calculated for four frequencies of 125Hz, 250Hz, 500Hz and 1000Hz at one horizontal line of receivers placed at 1.0 m above the ground, and in the second case, responses are computed in the common interface (Γ) between the sub-regions. A dual-BEM model is used as a reference model for comparison of the computed results. This model was discretized with a very large number of elements (about 50 elements per wavelength) to ensure the accuracy of the numerical solution. Here, the number of collocation points is defined by means of the relation between the incident wavelength and distance between collocation points. This relation is defined as r. The distance between the virtual sources and the fictitious circular interface is defined as D_{vs} and the distance of the collocation points is defined as D_{cp}. In all results, the number of virtual sources is equal to the number of collocation points.

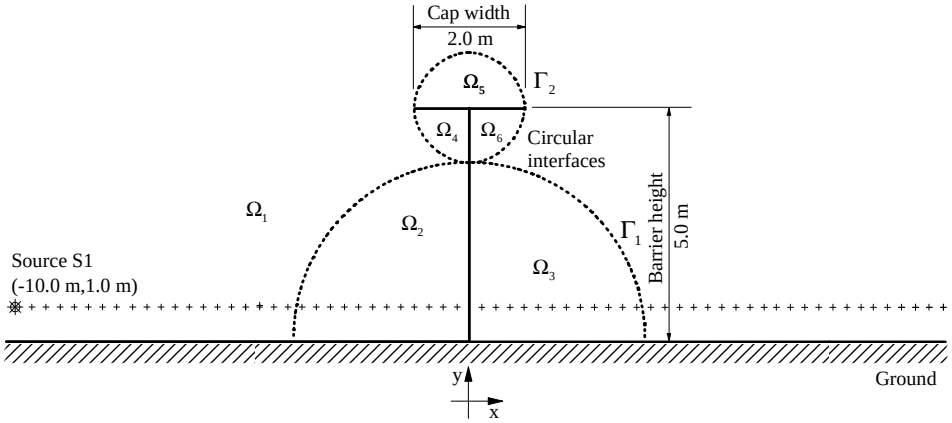

Figure 4. Schematic representation of the test cases.

The results in Figure 5(a1-d1), calculated for frequencies of 125Hz, 250Hz, 500Hz and 1000Hz, allow concluding that the MFS solution provides a very good approximation to the reference solution. To better understand the numerical behaviour of the MFS model, a global normalized error with respect to the reference solution was calculated as:

$$E = \frac{\sum_{i=1}^{nrec} \left| p_i^{\text{dual-BEM}} - p_i^{\text{MFS}} \right|}{\sum_{i=1}^{nrec} \left| p_i^{\text{dual-BEM}} \right|}, \tag{21}$$

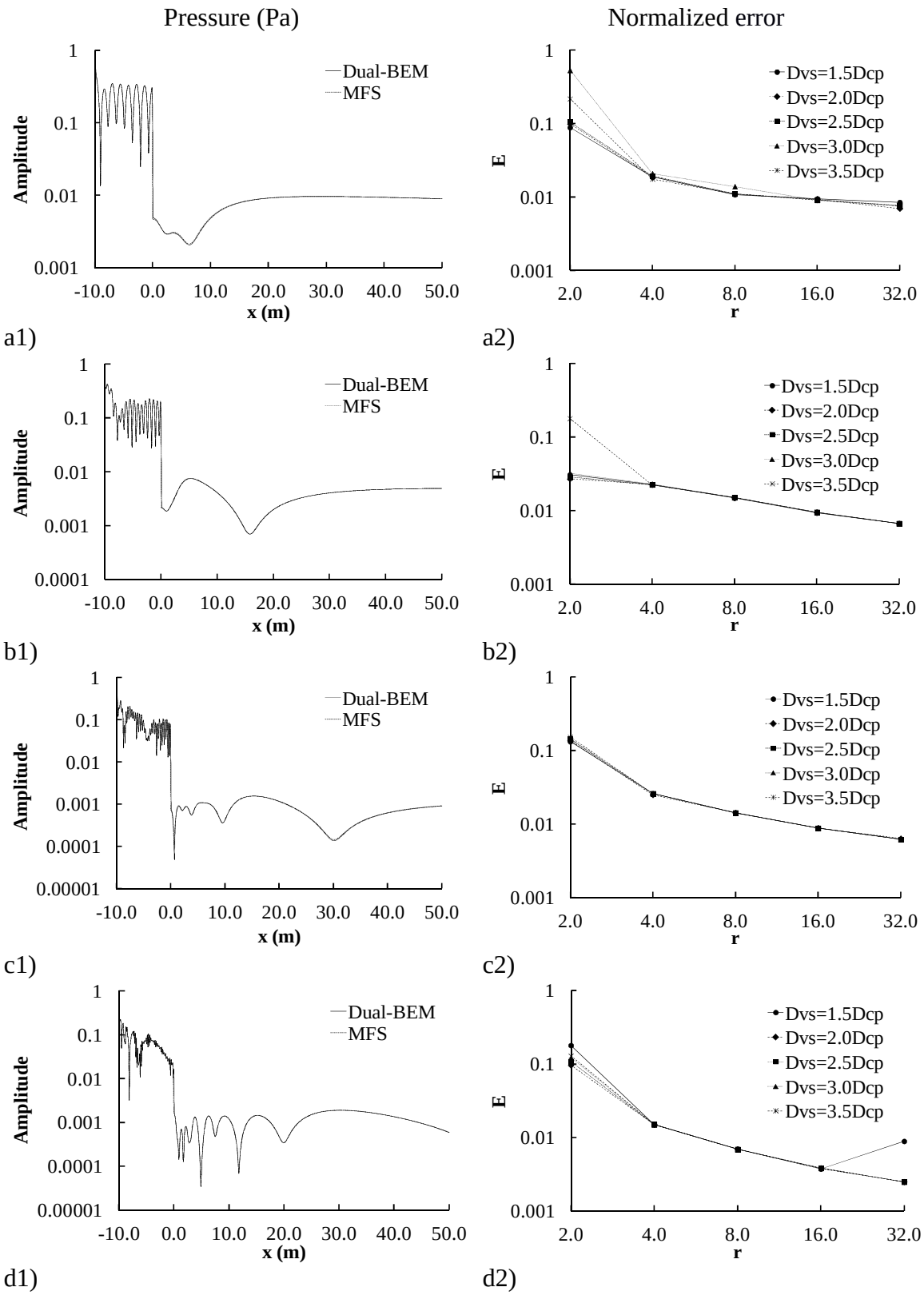

Figure 5. Responses along the horizontal line of receivers for the excitation frequencies of: a) 125Hz; b) 250Hz; c) 500Hz and d) 1000Hz.

for different values of the distance between the virtual sources and fictitious circular interfaces and for different relations. The results of theses computations are presented in Figs. 5(a2-d2), indicating that the MFS response converges to the reference solution as the relation *r* increases. This indicates the good stability of the proposed method with respect to the distance between the virtual sources and the fictitious circular interfaces.

Due to the variability of the response obtained by MFS based on the distance of the virtual sources and the fictitious interfaces of the problem, it becomes difficult to apply this method for problems when a more general case is considered or when the exact solution is not known. For this reason, several researchers have proposed strategies to solve this problem associated with the position of these virtual sources (Barnett, Betcke, 2008; Karageorghis, 2009). Therefore, a strategy proposed by Tadeu *et al*. (2009) is here used to assess the quality of the MFS responses by means of an integration along the interface of the problem through the difference between the responses computed in each sub-region, which can provide important information on the quality of the continuity conditions between the sub-regions, and thus can give a measurement of the error associated with the calculation. This strategy can be calculated by means of a global normalized integrated error given by:

$$\varepsilon = \frac{\int_{\Gamma} \left| p_{\Omega_1} - p_{\Omega_i} \right| d\Gamma}{\int_{\Gamma} \left| p_{\Omega_1} \right| d\Gamma}, \tag{22}$$

where p_{Ω_1} refers to the acoustic pressure of the sub-region Ω_1, p_{Ω_i} (with $i = 2,\ldots,6$) refers to the acoustic pressure from Ω_2 to Ω_6 and $\Gamma=\Gamma_1+\Gamma_2$ is the common interface between the sub-regions. Thus, a similar calculation is presented for different relations between the incident wavelength and distance between collocation points and for different distances between the virtual sources and the fictitious circular interfaces, for the frequencies of 125Hz, 250Hz, 500Hz and 1000Hz, with the aim of better describing the stability and the accuracy of the proposed method.

Figure 6(a1-d1) illustrates the acoustic pressure calculated at the circular interface Γ_1 (see Fig. 4). In the results presented, calculated by using the relation *r*=32.0 for all frequencies, and by assuming the virtual sources to be placed at $D_{vs}=2.0D_{cp}$ from the circular interfaces, there is an excellent match between the two responses. For the circular interface Γ_2, a good agreement between the two results was also found (not presented).

Figure 6(a2-d2) displays an integrated normalized error (ε) computed along the circular interface (Γ), which was evaluated using the approach described before. Notice that the error always decreases as the relation *r* increases. This convergent behaviour was found for all the distances analysed. These results suggest that the evaluation of the integral calculated at the interfaces continuity can be a very efficient strategy for assessing the quality of the MFS solution for problems when the analytical solution is not known and/or when a more general case is considered. In addition, this strategy allows identifying problems in the behaviour of the proposed MFS model.

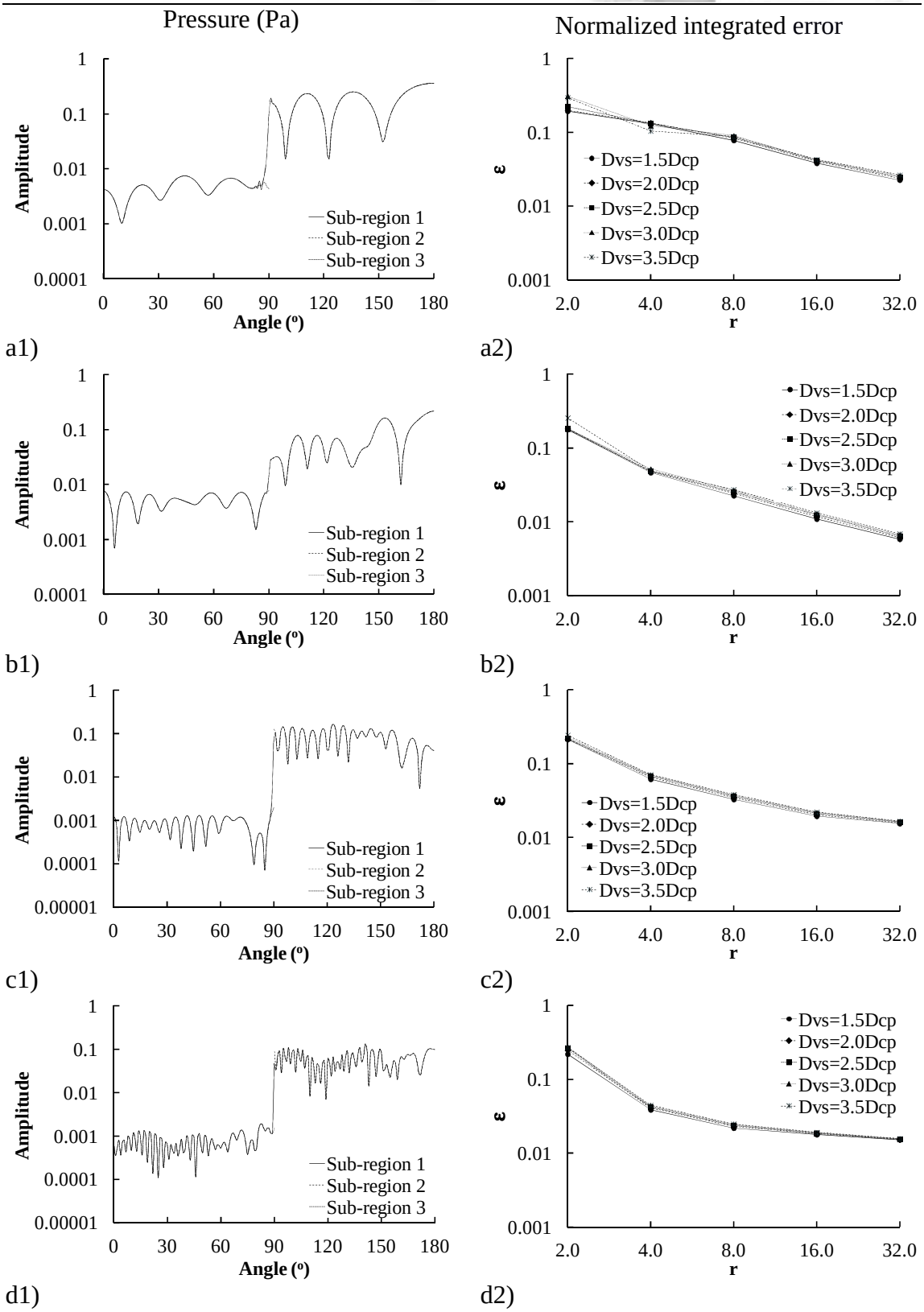

Figure 6. Responses along the circular interface (Γ_1) for the excitation frequencies of: a) 125Hz; b) 250Hz, c) 500Hz and d) 1000Hz.

It is important to note that in all the analyses, both the normalized and the integrated normalized errors clearly reveal a small error when a relation r=32.0 is considered. Thus, in the next section, the numerical examples will be analysed by using this relation to ensure the accuracy of the proposed method.

5 NUMERICAL EXAMPLES

In order to show the applicability of the MFS formulation, the problem illustrated in Fig. 7 is analysed in this section using T-shaped thin barriers in different scenarios. The simulations are analysed for four 1/3rd octave frequency bands of 125Hz, 250Hz, 500Hz and 1000Hz. These frequency bands are commonly used in traffic noise. In this analysis, an excitation source S1 is located at position (-10.0m, 0.7m) while another source S2 is located at position (-5.0m, 0.7m), and the T-shaped thin barriers are located at position (0.0m, 0.0m). Once again, the acoustic medium is assumed to be air at 20 ^{o}C and atmospheric pressure of 1 atm, with density of 1.21kg m^{-3} and sound propagation velocity of 343m s^{-1}. The Insertion Loss ($\mathrm{IL} = -20\mathrm{Log}_{10}\left(|p|/|p_0|\right)$ with p_0 being the acoustic pressure generated by a point source without the presence of the barrier) is used to show the influence of the T-shaped thin noise barrier above an infinite rigid ground. Here, the virtual sources are placed at D_{vs}=2.0D_{cp} from the circular interfaces and a relation r=32.0 was always used. In this example, the IL values are computed at a set of receivers located along a vertical line 0.5m away from the façade of a building, for the four 1/3rd octave frequency bands. Both the ground and the tall building are treated as infinite rigid plane surfaces. The upper surface of the cap is covered with a porous absorbent material. The properties of the porous material are c_s=3.0, Λ=0.3 and σ=10kPa s m^{-2}. Here, a barrier 5.0m tall with cap 1.0m width is used. This barrier is placed 20.0m from the building. In all the analyses, the responses provided by a T-shaped rigid barrier are displayed and used as a reference solution.

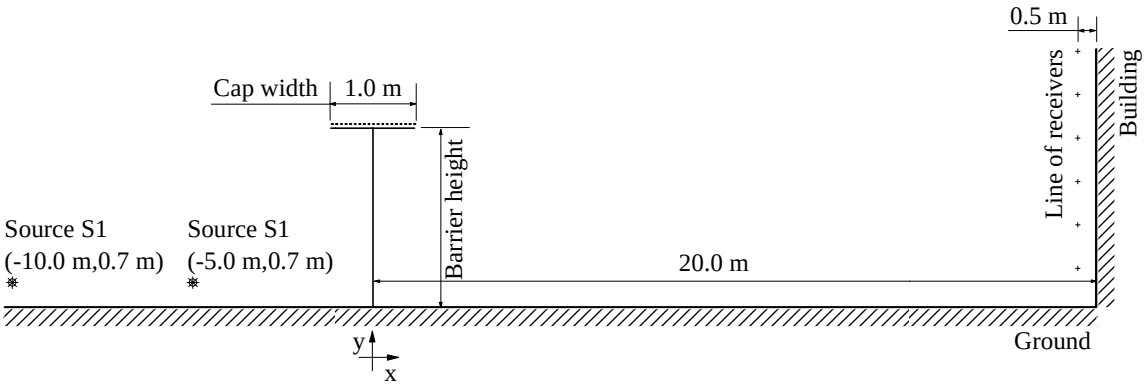

Figure 7. Geometry of the example.

Figure 8 illustrates the acoustic performance of a T-shaped thin barrier in the vicinity of tall buildings for the sources S1 and S2. In this analysis, a cap 1.0m width is assumed.

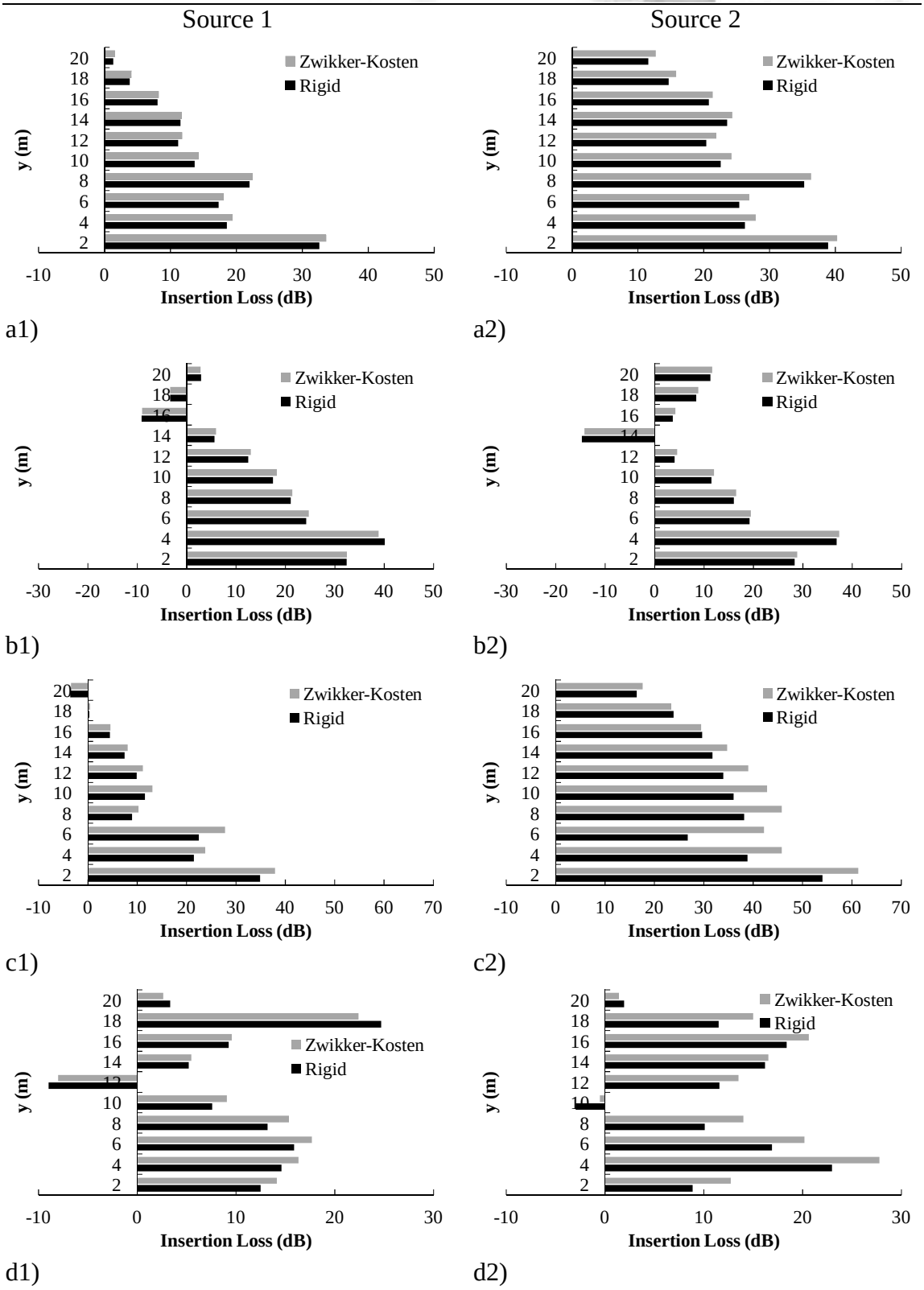

Figure 8. IL values at a set of receivers located along a vertical line 0.5 m away from the building, considering a cap 1.0m width, for the 1/3rd octave frequency bands of: a) 125Hz; b) 250Hz; c) 500Hz and d) 1000Hz.

Analyses of the results reveal increased IL values for the receivers placed near to the ground. These values are even more pronounced, when the source is at position 2, probably due to increase of the shadow zone. The barriers with absorbent treatment provide better results than the rigid barriers. The performance of the absorptive barrier improves as receivers are placed closer from the ground. However, an exception of this behaviour can be observed for the frequency band of 250Hz at y=4.0m (see Fig. 8(b1)). After reaching the maximum performance, all barriers become less efficient as the distance to the ground increases and thus negative IL values may also be registered. These negative values are more pronounced for the lower frequency band of 250Hz at y=16.0m and at y=14.0m (see Figs. 8(b1) and (b2), respectively), and for the higher frequency band of 1000Hz at y=12.0m (see Fig. 8(d1)), leading to the enhancement of the sound pressure level next to the façade of the buildings.

6 CONCLUSIONS

In this paper, a two-dimensional numerical model based on Method of Fundamental Solutions was used to simulate acoustic pressure field produced by a point source in the presence of a T-shaped thin barrier. In the numerical model, both the ground and the façade of a building were treated as infinite rigid plane surfaces, and the barriers were assumed to be absorptive. This model made use of Green's functions defined by the image-source technique, limiting the number of discretized surfaces and reducing the computational cost of the proposed model. This model was verified by comparing the results with a reference model based on the dual-BEM formulation. The results analysed in this work further revealed convergence of the proposed method to the reference solution when the number of collocation points and virtual sources was increased, and the good stability of the solution with respect to the distance between virtual sources and the fictitious circular interface between sub-regions. The acoustic insertion loss was presented for barriers with and without absorbent treatment, showing the effect of the absorbent treatment of the barriers in the sound reduction next to the façade of tall buildings. This analysis makes it clear that the MFS is a very interesting tool for problems of thin acoustic barriers with complex shapes and complicated boundary conditions.

ACKNOWLEDGEMENTS

The financial support by CNPq and PNPD/CAPES is greatly acknowledged. This work was partly supported by FEDER funds through the Competitivity Factors Operational Programme - COMPETE and by national funds through FCT – Foundation for Science and Technology within the scope of the project POCI-01-0145-FEDER-007633 and through the Regional Operational Programme CENTRO2020 within the scope of the project CENTRO-01-0145-FEDER-000006.

REFERENCES

Brebbia, C. A., 1984. *The Boundary Element Method for Engineers*. Pentech Press, London.

Barnett, A. H., & Betcke, T., 2008. Stability and Convergence of the Method of Fundamental Solutions for Helmholtz Problems on Analytic Domains, *Journal of Computational Physics*, vol. 227, pp. 7003-7026.

Cassot, F., 1975. Contribuition à L'étude de la Diffraction par un Écran Mince, *Acoustic*, vol. 34, pp. 64-71.

Costa, E. G. A., Godinho, L., Santiago, J. A. F., Pereira, A., & Dors, C. 2011. Efficient Numerical Models for the Prediction of Acoustic Wave Propagation in the Vicinity of a Wedge Coastal Region, *Engineering Analysis with Boundary Elements*, vol. 35, pp. 855-867.

Costa, E. G. A., Godinho, L., Pereira, A., & Santiago, J. A. F., 2012. Prediction of Acoustic Wave Propagation in a Shallow Water Configuration using The Method of Fundamental Solutions, *Journal of Computational Acoustics*, vol. 20, n. 4, 1250013.

Costa, E. G. A., Santiago, J. A. F., Godinho, L., Wrobel L. C, & Mansur W., 2016. Three Efficient Numerical Models to Analyse the Step Problem in Shallow Water, *Engineering Analysis with Boundary Elements*, vol. 62, pp. 44-56.

Costa, E. G. A., Godinho, L., Santiago, J. A. F., & Mansur W., 2018. Efficient Model for Acoustic Attenuators using the Method of Fundamental Solutions, *International Journal of Acoustics and Vibration*, vol. 23, n. 1, pp. 74-82.

Filippi, P., & Dumery, G., 1969. Etude Théorique et Numérique de la Diffraction par un Écran Mince. *Acustica*, vol. 21, pp. 343-359.

Godinho, L. M. C., Costa, E. G. A., Pereira, A. S. C., & Santiago, J. A. F., 2012. Some Observations on the Behavior of the Method of Fundamental Solutions in 3D Acoustic Problems, *International Journal of Computational Methods*, vol. 9, n. 4, 1250049.

Kawai, Y., & Terai, T., 1990. The Application of Integral Equation Methods to the Calculation of Sound Attenuation by Barriers, *Applied Acoustics*, vol. 31, pp. 101-117.

Karageorghis, A., 2009. A Practical Algorithm for Determining the Optimal Pseudo-Boundary in the Method of Fundamental Solutions, *Advances in Applied Mathematics and Mechanics*, vol. 1, n. 4, pp. 510-528.

Tadeu, A., António, J., & Godinho, L., 2009. Defining an Accurate MFS Solution for 2.5D Acoustic and Elastic Wave Propagation, *Engineering Analysis with Boundary Elements*, vol. 33, pp. 1383-1395.

Salomons, E.M., 2001. *Computational Atmospheric Acoustics*, Kluwer Academic Pub., Dordrecht.